Changes in Geometries and Spin States of Thiolato–Schiff Base NiN_2S_2 Complexes Containing *N,N'*-Biphenyl Backbones

Henrik Frydendahl,[†] Hans Toftlund,*[,†] Jan Becher,[†] Jennifer C. Dutton,[‡] Keith S. Murray,*[,‡] Lucille F. Taylor,[§] Oren P. Anderson,[§] and Edward R. T. Tiekink[||]

Departments of Chemistry, Odense University, DK-5230, Odense M, Denmark, Monash University, Clayton, Victoria 3168, Australia, Colorado State University, Fort Collins, Colorado 80523, and University of Adelaide, Adelaide, South Australia 5001, Australia

Received September 30, 1994[⊗]

Four new 5-formylpyrazole-based thiolato Schiff base nickel(II) complexes (**1**–**4**) have been synthesized from the corresponding ligands and nickel(II) acetate. A new 2-mercaptobenzaldehyde Schiff base nickel(II) complex (**5**) has been synthesized by two routes. X-ray structural analyses on three of the complexes showed the following: **1**, chemical formula $C_{26}H_{26}N_6S_2Ni$, monoclinic, space group $P2_1/n$ with $a = 10.438(2)$ Å, $b = 12.450(3)$ Å, $c = 19.616(3)$ Å, $\beta = 94.33(1)°$, $Z = 4$, and $R = 0.044$ for 3365 reflections; **4**, chemical formula $C_{34}H_{26}N_6S_2Ni$, monoclinic, space group $C2/c$ with $a = 19.242(3)$ Å, $b = 9.757(2)$ Å, $c = 19.691(3)$ Å, $\beta = 125.84(1)°$, $Z = 4$, and $R = 0.032$ for 2206 reflections; **5**, chemical formula $C_{28}H_{22}N_2S_2Ni$, monoclinic, space group $C2/c$ with $a = 25.230(4)$ Å, $b = 11.098(2)$ Å, $c = 17.287(8)$ Å, $\beta = 98.46(3)°$, $Z = 8$, and $R = 0.047$ for 1912 reflections. The coordination geometry in **1** is distorted tetrahedral while in **4** and **5** it is close to *cis*-square planar despite the influence of the (6,6'-dimethyl)biphenyl group in the tetradentate ligand backbone. The bond distances are as follows. Ni–S: **1**, 2.239(1), 2.243(1) Å; **4**, 2.185(1) Å; **5**, 2.152(2), 2.184 (2) Å. Ni–N: **1**, 1.963(2), 1.968(2) Å; **4**, 1.927(2); **5**, 1.931(5), 1.917(6) Å. The distortions from tetrahedral to planar geometry are manifest in some interesting changes in dihedral angles and donor atom "bite" distances. The magnetic susceptibilities were measured in the temperature range 4.2–300 K for **1**–**5**. The susceptibilities of **1** and **2** could be fitted well to a simple axial spin Hamiltonian with $S = 1$, $D = 34$ cm^{-1} and $S = 1$, $D = 53$ cm^{-1}, respectively. Complexes **3**–**5** are diamagnetic and showed only small temperature-independent paramagnetic susceptibilities. Although no temperature-induced spin changes were observed for solids of **1**–**4**, they all showed a $^1A_{1g} \rightleftarrows {}^3T_1$ equilibrium in chloroform solutions. Each of complexes **1**–**5** show LF, CT, and intraligand spectral features in the spectral region 5,000 - 40,000 cm^{-1}. Bands assigned to the high-spin and low-spin forms are observed separately. The thermodynamic parameters for the high-spin $\rightleftarrows$ low-spin equilibria in chloroform solutions were obtained by using the Evans method, variable-temperature ^{1}H NMR spectra, and variable-temperature electronic spectra. Complexes **1**–**4** exhibit equilibrium constants K_{eq} ($=N_{HS}/N_{LS}$) in the range of 0.456–0.080.

Introduction

There is much current interest in the use of distorted MN_2S_2 complexes as structural and spectroscopic models for the active site coordination environments of a number of metalloproteins. For example, in our work on the preparation of pseudotetrahedral $Cu^{II}N_2S_2$ Schiff base complexes[1,2] as models for the "visible" copper site (Cu_A) in cytochrome *c* oxidase and of the Zn^{II} analogues[3] as models for LADH and other zinc enzymes, we have demonstrated that the necessary twist in the resulting complex can be introduced by using a biphenyl moiety as a backbone in the ligand. Furthermore, by employing heterocycles such as pyrazolethiols as building blocks, we have been able to vary both the geometry of the ligand and the electron density of the donor atoms in the resulting N_2S_2 metal complexes. In the present paper, we apply these tactics to a series of NiN_2S_2 complexes and suggest below that the results may be relevant to an understanding of the role of nickel in the active sites of cysteine-coordinated nickel metalloproteins.

In 1957, Lions and co-workers[4] reported the use of a biphenyl backbone for the control of geometry in complex chemistry. Holm and co-workers[5,6] subsequently used the same backbone in a series of salicylaldimine NiN_2O_2 complexes analogous to some of the complexes described herein and employed ^{1}H NMR techniques to monitor the planar $\rightleftarrows$ tetrahedral equilibrium in solution. Recently, Schugar and co-workers[7] have used the biphenyl backbone for controlling the geometry in a series of bis(imidazolyl) MN_4 complexes ($M^{II} = Cu^{II}$, Ni^{II}, Co^{II}, Zn^{II}). These authors noted that ligand field effects in Ni^{II} and Cu^{II} complexes would tend to distort complexes toward planar geometries and that use of biphenyl backbones could counteract this. Müller *et al.*[8] subsequently studied Cu^I and Cu^{II} complexes of a bis-bipyridyl-biphenyl ligand system.

We have endeavored to test the effect of some of these ligand design/constraint features in a series of neutral four-coordinate imino–thiolato NiN_2S_2 complexes of the type shown in Figure

[†] Odense University.
[‡] Monash University.
[§] Colorado State University.
[||] University of Adelaide.
[⊗] Abstract published in *Advance ACS Abstracts,* July 15, 1995.

(1) Anderson, O. P.; Becher, J.; Frydendahl, H.; Taylor, L. F.; Toftlund, H. *J. Chem. Soc., Chem. Commun.* **1986**, 699.
(2) Toftlund, H.; Becher, J.; Olesen, P. H.; Pedersen, J. Z. *Isr. J. Chem.* **1986**, *25*, 56.
(3) Frydendahl, H.; Becher, J.; Toftlund, H.; Dutton, J. C.; Murray, K. S.; Taylor, L. F.; Anderson, O. P.; Tiekink, E. R. T. To be submitted for publication.
(4) Lions, F.; Martin, K. V. *J. Chem. Soc.* **1957**, 127.
(5) O'Connor, M. J.; Holm, R. H. *Prog. Inorg. Chem.* **1971**, *14*, 241.
(6) O'Connor, M. J.; Ernst, R. E.; Holm, R. H. *J. Am. Chem. Soc.* **1968**, *90*, 4561.
(7) Knapp, S.; Keenan, T. P.; Zhang, X.; Fikar, R.; Potenza, J. A.; Schugar, H. J. *J. Am. Chem. Soc.* **1987**, *109*, 1882.
(8) Müller, E.; Piquet, C.; Bernadinelli, G.; Williams, A. F. *Inorg. Chem.* **1988**, *27*, 849.

0020-1669/95/1334-4467$09.00/0

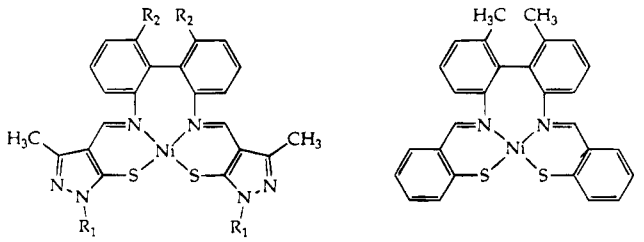

Figure 1. Schematic representation of the structures of complexes **1**–**4** (left) and **5** (right). For **1**–**4**, substituents are as follows: for **1**, $R_1 = R_2 = CH_3$; for **2**, $R_1 = CH_3$, $R_2 = H$; for **3**, $R_1 = C_6H_5$, $R_2 = CH_3$; for **4**, $R_1 = C_6H_5$, $R_2 = H$.

1. Complexes **1**–**4** contain a substituted pyrazole group fused to the six-membered chelate ring, while complex **5** incorporates a benzene ring in this portion and is analogous to the salicylaldimine systems of Holm *et al.*[6] We were particularly interested in monitoring spin state changes in the crystalline complexes and spin equilibria in solution for these complexes and, where possible, relating any observed changes to structural and electronic effects. Magnetic susceptibility studies have been used in combination with UV–visible and ^{1}H NMR spectroscopies to achieve these aims.

In the general context of Schiff base NiN_2S_2 chemistry it should be noted that tetradentate chelates of both the pyrazolylimine and benzaldimine types containing alkyldiimine backbones have been studied over the past 25 years, as have the bis-bidentate analogues. Indeed, some of the present authors first studied the *N,N'*-ethylene-based system commonly referred to as Ni(tsalen) and bis-bidentate derivatives ($Ni(mb\text{-}NR)_2$) in the late 1960's; recently, the R = Bu^t complex has been structurally characterized,[9] as has the Ni(tsalen) complex.[10] The structures and NMR spectra of other nickel complexes and analogous complexes based on heterocyclic aldimines are presently emerging from our laboratories[11] and from the extensive studies on such systems carried out by the group of Minkin *et al.*[12,13] Systematic studies on related tetradentate NiN_2S_2 systems have been reported by Bereman *et al.*,[14,15] and those on NiN_4 "tropocoronands" by Lippard *et al.*[16]

Other non-Schiff base *cis*-N_2S_2 complexes of Ni^{II} (and Ni^{III}) are also receiving much attention. Holm and co-workers[17] have recently found that tetradentate amido thiolate ligands, in their fully deprotonated (4−) forms, can stabilize both oxidation states, thus making these planar compounds useful redox and spectroscopic models for bioinorganic nickel systems such as [NiFe]-hydrogenases (*e.g.*, from *Desulfovibrio gigas*).[18] While the present compounds do not provide the desired low $Ni^{III/II}$ redox potentials appropriate to hydrogenase enzymes,[17] they do provide an excellent molecular system in which to systematically vary electronic and structural facets of the ligand environment. In particular, variations in the distortion from planar to tetrahedral geometries within a closely matched N_2S_2 ligand environment are possible, thus allowing quantitative measurements of relevant spectroscopic, magnetic, and thermodynamic parameters.

As intimated earlier, studies of the present kind will aid in a better understanding of the active site environment of N,S-coordinated nickel enzymes and of Ni-substituted metalloproteins. Recent papers on EXAFS[19] and XANES[20] studies of [NiFe]-hydrogenase enzymes (e.g., from *Thiocapsa roseopersicina*[20]) and on model complexes show that nickel appears to be coordinated to S, N, and O donors, possibly in a distorted five-coordinate arrangement.

Experimental Section

Physical Measurements. Elemental analyses were carried out at Copenhagen University and the National Analytical Laboratory, Melbourne. Mass spectra were recorded on Varian MAT311A and VG-Micromass 7070F spectrometers. IR spectra were recorded from 450 to 4000 cm^{-1} in KBr disks or as Nujol mulls on a Perkin-Elmer 1720 FTIR spectrometer. UV–visible spectra were recorded from 240 to 2000 nm in chloroform (AR grade) on a Cary 1756 spectrometer.

^{1}H NMR spectra were recorded on Bruker AC200 and Bruker AM300 spectrometers with standard variable-temperature equipment, $CDCl_3$ as solvent, and tetramethylsilane as internal reference. During the variable-temperature measurements of isotropic shifts the temperatures were checked by measuring the shifts of a methanol sample.

The theoretical expressions for the isotropic shift, $\Delta H_i/H_0$, occurring in a chelated nickel(II) complex undergoing a planar $\rightleftarrows$ tetrahedral configurational equilibrium have been given elsewhere[5,21] and are briefly summarized below. The contact shift for a proton in two isomers undergoing rapid conversion is an average shift of the form

$$-\left(\frac{\Delta H_i}{H_o}\right)_{cont} = \frac{\Delta\nu}{\nu_0} = \frac{\Delta\nu(\text{obs})}{\nu_0} - \frac{\Delta\nu(\text{diamag})}{\nu_o} = A_i\left(\frac{2\pi}{\gamma_H}\right)\frac{g\beta S(S+1)}{3kT}(\exp(\Delta G/RT)+1)^{-1}$$

where $R = 8.31441$ J K^{-1} mol^{-1}, $k = 1.38066 \times 10^{-16}$ erg K^{-1}, $\beta = 9.2732 \times 10^{-21}$ erg G^{-1}, and $\gamma_H = 2.6752 \times 10^4$ s^{-1} G^{-1}. The last term in the equation represents the mole fraction of the tetrahedral high-spin form, N_{HS}. Here $\Delta G = -RT \ln K_{eq}$, and $K_{eq} = N_{HS}/N_{LS}$, where N_{LS} is the mole fraction of the planar, low-spin isomer. To obtain ΔG, the g values and the A_i values (electron nuclear hyperfine coupling constants) for the $S = 1$ (HS) forms are required. From complexes **1** and **2**, $g = \mu_{eff}[S(S+1)]^{-1/2} = 3.055 \times 2^{-1/2} = 2.16$ (average). The A_i values can be obtained from the variable-temperature plots of $\Delta\nu/\nu_0$ (ppm) versus $1/T$ by using the following expression:

$$A_i = 4.4018 \times 10^7 \times \Delta\nu/\nu \times T \times \{\exp(\Delta G/RT) + 1\}$$

The thermodynamic parameters may then be obtained by combining this equation with the following expression:

$$\ln K_{eq} = -\frac{\Delta H}{RT} + \frac{\Delta S}{R} = -\ln\left\{\frac{\nu_0}{\Delta\nu}\left(\frac{A_i 2\pi g S(S+1)}{3kT}\right) - 1\right\}$$

Magnetic Susceptibilities. Measurements at room temperature on the solids were made by using a Faraday balance incorporating a Newport 4-in. electromagnet fitted with Faraday pole pieces and a Cahn RG electrobalance. The instrument was calibrated with

(9) Marini, P.; Murray, K. S.; Tiekink, E. R. T.; West, B. O. to be published.
(10) Yamamura, T.; Tadokoro, M.; Kuroda, R. *Chem. Lett. (Jpn.)* **1989**, 1245.
(11) la Cour, A.; Adhikary, B.; Toftlund, H.; Hazell, A. *Inorg. Chim. Acta* **1992**, *202*, 145.
(12) Nivorozhkin, A. L.; Nivorozhkin, L. E.; Minkin, V. L.; Takhirov, T. G.; Diachenko, O. A. *Polyhedron* **1991**, *10*, 179 and see references therein.
(13) Garnovskii, A. D.; Nivorozhkin, A. L.; Minkin, V. I. *Coord. Chem. Rev.* **1993**, *126*, 1.
(14) Martin, E. M.; Bereman, R. D.; Singh, P. *Inorg. Chem.* **1991**, *30*, 957.
(15) (a) Martin, E. M.; Bereman, R. D.; Dorfman, J. R. *Inorg. Chim. Acta* **1990**, *176*, 247. (b) Martin, E. M.; Bereman, R. D. *Inorg. Chim. Acta* **1991**, *188*, 221. (c) Martin, E. M.; Bereman, R. D. *Inorg. Chim. Acta* **1991**, *188*, 233.
(16) Davis, W. M.; Roberts, M. M.; Zask, A.; Nakanishi, K.; Nozoe, T.; Lippard, S. J. *J. Am. Chem. Soc.* **1985** *107*, 3864.
(17) Krüger, H.-J.; Peng, G.; Holm, R. H. *Inorg. Chem.* **1991**, *30*, 731.
(18) (a) Lancaster, J. R., Ed. *The Bioinorganic Chemistry of Nickel*; VCH Publishers Inc.: New York, 1988. (b) Kolodziej, A. F. *Prog. Inorg. Chem.* **1994**, *41*, 493. (c) Cammack, R. In *Bioinorganic Catalysis*; J., Reedijk, Ed.; Marcel Dekker Publishers: New York, 1993; p 189.
(19) Scott, R. A.; Czechowski, M.; DerVartanian, D. V.; LeGall, J.; Peck, H. D., Jr.; Moura, I. *Rev. Port. Quim.* **1985**, *27*, 67.
(20) (a) Colpas, G. J.; Maroney, M. J.; Bagyinka, C.; Kumar, M.; Willis, W. S.; Suib, S. L.; Baidya, N.; Mascharak, P. K. *Inorg. Chem.* **1991**, *30*, 920. (b) Baidya, N.; Olmstead, M. M.; Mascharak, P. K. *J. Am. Chem. Soc.* **1992**, *114*, 9666.
(21) Holm, R. H.; Hawkins, C. J. In *NMR of Paramagnetic Molecules*; LaMar, G. N., Horrocks, W. de W., Jr., Holm, R. H., Eds.; Academic Press: New York, 1973; p 243.

$CuSO_4 \cdot 5H_2O$ and $Hg[Co(NCS)_4]$. Variable temperature measurements on the solids were made by using an Oxford Instruments Faraday magnetometer with a superconducting magnet and Hewlett-Packard automated data acquisition electronics.[22] A main field of 10 kOe and a gradient field of 1000 Oe cm^{-1} were employed. Solution susceptibilities were determined on $CDCl_3$ solutions (+1% TMS) by Evans' method[23] employing the equation

$$\chi_g = \frac{3\Delta\nu}{4\pi\nu_0 c} + \chi_0 + \frac{(d_0^{293} - d_s^{293})}{c^{293}}\chi_0$$

Particular attention was paid to obtaining the third term, which allows for density differences (χ_g = gram susceptibility of the dissolved complex, $\Delta\nu$ = frequency separation between the two methyl resonances, ν_0 = spectrometer frequency, c = concentration, χ_0 = solvent susceptibility, d_0^{293} = solvent density, d_s^{293} = solution density). Susceptibilities were corrected for the diamagnetism of the appropriate ligand by using Pascal's constants. In the spin-equilibrium systems, the equilibrium constants were obtained from the magnetic moments by use of the relationships

$$K_{eq} = \frac{\mu_{obs}^2 - \mu_{LS}^2}{\mu_{HS}^2 - \mu_{obs}^2} = \frac{N_{HS}}{N_{LS}}$$

$$N_{HS} = \frac{K_{eq}}{1 + K_{eq}}$$

Synthesis of Ligands and Complexes. The pyrazole-based ligands, their bis(*tert*-butyl thioether) precursors, and 2,2′-diamino-6,6′-dimethylbiphenyl were prepared as described elsewhere.[3] 2-Mercaptobenzaldehyde was prepared as described previously.[24]

Complex **1** was prepared by refluxing the *S-tert*-butyl-protected derivative of the corresponding ligand[3] (0.30 g, 0.50 mmol) with $NiCl_2 \cdot 6H_2O$ (0.15 g, 0.63 mmol) in 2-methoxyethanol (12 mL) for 1 h. After reduction of volume *in vacuo*, ethanol (10 mL) and 3 drops of triethylamine were added. After standing for 1 h, dark brown crystals were isolated by filtration. Yield: 0.09 g (33%). Anal. Calcd for $C_{26}H_{26}N_6S_2Ni$: C, 57.26; H, 4.81; N, 15.41; S, 11.76. Found: C, 56.16; H, 5.38; N, 14.37; S 9.36. MS: *m/e* 543.8 (100%, M^+), 390.8 (21%), 299.9 (45%), 271.9 (8%, M^{2+}); peaks at lower *m/e* values had intensities below 7%.

Complex **2** was prepared by mixing a solution of the corresponding ligand[3] (0.46 g, 1.0 mmol) in chloroform (10 mL) with a solution of nickel(II) acetate tetrahydrate (0.26 g, 1.0 mmol) in absolute ethanol (8 mL). The volume of the resulting dark solution was reduced *in vacuo*, whereupon a dark green solid precipitated. This was filtered out, washed twice with absolute ethanol, and dried *in vacuo* at room temperature. Yield: 0.47 g (90%). Anal. Calcd for $C_{24}H_{22}N_6S_2Ni$: C, 55.72; H, 4.29; N, 16.25. Found; C, 54.96; H, 4.21; N, 15.83. MS: *m/e* 516 (100%, M^+), 363 (18%), 304 (4%), 272 (45%), 258 (11%, M^{2+}); peaks at lower *m/e* values had intensities below 5%.

Complex **3** was prepared as described for **2**. Yield 98%; olive green needles. Anal. Calcd for $C_{36}H_{30}N_6S_2Ni$: C, 64.59; H, 4.52; N, 12.55. Found: C, 63.44; H, 4.47; N, 12.17. MS: *m/e* 668 (100%, M^+), 453 (7%), 362 (43%), 334 (12%, M^{2+}); peaks at lower *m/e* values had intensities below 8%.

Complex **4** was prepared as described for **2**: Yield 78%; olive green powder. Anal. Calcd for $C_{34}H_{26}N_6S_2Ni$: C, 63.66; H, 4.09; N, 13.10; S, 10.00. Found: C, 62.34; H, 4.22; N, 12.86; S, 9.69. MS: *m/e* 640 (100%, M^+), 425 (7%), 366 (12%), 334 (50%), 320 (17%, M^{2+}), 293 (10%); peaks at lower *m/e* values had intensities below 8% except for *m/e* 77 (15%) and 43 (20%).

Complex **5** was prepared by two routes. In the first route, a diethyl ether solution of 2-mercaptobenzaldehyde[24] (0.14 g, 1.0 mmol) was added with stirring to a warm ethanolic solution of nickel(II) acetate tetrahydrate (0.13 g, 0.52 mmol). After 15 min a solution of 2,2′-diamino-6,6′-dimethylbiphenyl (0.16 g, 0.75 mmol) in ethanol (25 mL) was added and the mixture was refluxed for a further 15 min. On cooling a small amount of brown solid (bis(2-mercaptobenzaldehydato)-nickel(II)) was deposited; this side product (yield 0.03 g (18%); MS *m/e* 332 (5%, M^+), 300 (2%), 242 (2%), 216 (50%), 138 (40%), 110 (100%), 104 (25%); IR (Nujol mull, ν(C=O) region) 1600 cm^{-1} (sh), 1590 (s), 1520 (m)) was removed by filtration. After standing for several days, fine dark brown crystals of **5** had formed from the red-brown solution: Yield 0.02 g (7%); mp 320–322 °C. Anal. Calcd for $C_{28}H_{22}N_2S_2Ni$: C, 66.0; H, 4.4; N, 5.5. Found: C, 65.8; H, 4.6; N 5.7. MS: *m/e* 508 (100%, M^+), 476 (9%), 373 (9%), 282 (80%), 268 (15%), 121 (10%). IR (Nujol mull, ν(C=O) region): 1610 cm^{-1} (m), 1590 (s), 1570 (m), 1530 (m). A white suspension also formed (possibly a dithiocine derivative[25]), but this could easily be decanted away from the crystals of **5**. After filtration, the resulting solution was concentrated *in vacuo* to give a further 28% yield of **5**.

In the second route, an ethanolic solution (20 mL) of 2,2′-diamino-6,6′-dimethylbiphenyl (0.13 g, 0.61 mmol) was added to a diethyl ether solution of 2-mercaptobenzaldehyde (0.17 g, 1.2 mmol) chilled to ice bath temperature. The resulting red solution was stirred for 30 min, concentrated *in vacuo*, and added to a solution of nickel(II) acetate tetrahydrate (0.15 g, 0.60 mmol) in absolute ethanol (40 mL). On standing overnight 0.05 g (16%) of **5** deposited, and a further 0.06 g (19%) of well-formed brown crystals could be obtained on concentration of the filtrate. These crystals were used for the X-ray diffraction study. Recrystallization of **5** from 2-methoxyethanol also yielded crystals of good diffracting quality.

Table 1. Crystallographic Data for Complexes **1**, **4**, and **5**

compd	**1**	**4**	**5**
formula	$C_{26}H_{26}N_6S_2Ni$	$C_{34}H_{26}N_6S_2Ni$	$C_{28}H_{22}N_2S_2Ni$
fw	545.3	641.4	509.3
space group	$P2_1/n$ (No. 14)	$C2/c$ (No. 15)	$C2/c$ (No. 15)
a, Å	10.438(2)	19.242(3)	25.230(4)
b, Å	12.450(3)	9.757(2)	11.098(2)
c, Å	19.616(3)	19.691(3)	17.287(8)
β, deg	94.33(1)	125.84(1)	98.46(3)
Z	4	4	8
V, Å^3	2541.8	2996.9	4787.7
T, °C	22	20	20
λ, Å	0.710 73	0.710 73	0.710 73
ϱ_{calcd}, g cm^{-3}	1.425	1.422	1.413
μ, cm^{-1}	9.55	8.22	9.68
no. of unique rflns	4498	2578	4001
criterion of observn			$I \geq 2.5\sigma(I)$
no. of rflns in refinement	4498	2578	1912
R	0.061[a]	0.039[a]	0.047[a]
R_w	0.133[b]	0.107[b]	0.051[c]

[a] $R(F_o) = \sum||F_o| - |F_c||/\sum|F_o|$. [b] $R_w(F_o^2) = [\sum\{w(F_o^2 - F_c^2)^2\}/\sum\{w(F_o^2)^2\}]^{1/2}$; $w = [\sigma^2(F_o)^2 + (0.1000P)^2 + 0.0000P]^{-1}$, where $P = (F_o^2 + 2F_c^2)/3$. [c] $R_w(F_o) = [\{\sum w(F_o - F_c)^2\}/\{\sum wF_o^2\}]^{1/2}$; $w = [\sigma^2(F_o) + 0.007F_o^2]^{-1}$.

X-ray Crystallographic Studies. Intensity data for a dark brown prismatic crystal of **1** (0.34 × 0.30 × 0.20 mm) and an olive green prismatic crystal of **4** (0.32 × 0.14 × 0.22 mm) were measured at Colorado State University on a Siemens R3m diffractometer operating at room temperature and employing Mo Kα radiation (graphite monochromator, λ = 0.7107 Å). Bisecting geometry was used throughout the data collection. Data were measured to a maximum Bragg angle θ of 25.05° for both complexes; no significant decomposition of the crystals occurred during the data collection. No absorption corrections were carried out since the absorption coefficients were relatively small and the crystals were not extremely uneven in their dimensions. Details of the crystallographic experiments and the structural calculations are briefly summarized in Table 1.

The structures of **1** and **4** were solved by direct methods, and the SHELXTL-Plus software package[26] was used in all structural calculations. The structures were refined by a full-matrix least-square procedure based on F^2, using the SHELXL-93 part of the package. All reflections were used in the refinements for **1** and **4**. Hydrogen atoms were allowed to ride on the attached heavier atoms, being re-idealized on each cycle of refinement. Hydrogen atom thermal displacement

(22) Kennedy, B. J.; Murray, K. S. *Inorg. Chem.* **1985**, *24*, 1552.
(23) Evans, D. F. *J. Chem. Soc.* **1959**, 2003.
(24) Marini, P.; Murray, K. S.; West, B. O. *J. Chem. Soc., Dalton Trans.* **1983**, 143.
(25) (a) Corrigan, M. F.; Rae, I. D.; West, B. O. *Aust. J. Chem.* **1978**, *31*, 587. (b) Corrigan, M. F.; West, B. O. *Aust. J. Chem.* **1976**, *29*, 1413.
(26) Sheldrick, G. M. SHELXTL PLUS, Siemens Analytical X-ray Instruments, Madison, WI, 1990.

Table 2. Fractional Atomic Coordinates and Equivalent Isotropic Displacement Parameters ($Å^2 \times 10^3$) for **1**[a]

atom	*x*	*y*	*z*	U_{eq}[b]
Ni	0.2755(1)	0.1877(1)	0.6628(1)	43(1)
S(1)	0.1495(1)	0.1349(1)	0.5715(1)	48(1)
S(2)	0.1799(1)	0.2349(1)	0.7569(1)	52(1)
N(1)	0.3801(2)	0.2964(2)	0.6204(1)	36(1)
N(2)	0.4204(2)	0.1037(2)	0.7049(1)	38(1)
N(3)	0.2823(3)	0.0766(2)	0.9245(1)	48(2)
N(4)	0.2139(3)	0.1503(2)	0.8837(1)	44(2)
N(5)	0.1544(3)	0.3111(2)	0.4069(1)	50(2)
N(6)	0.1144(2)	0.2296(2)	0.4475(1)	45(2)
C(1)	0.2522(3)	0.1549(2)	0.8199(2)	38(2)
C(2)	0.3545(3)	0.0819(2)	0.8188(2)	38(2)
C(3)	0.3674(3)	0.0368(3)	0.8855(2)	42(2)
C(4)	0.4362(3)	0.0638(3)	0.7657(2)	41(2)
C(5)	0.1814(3)	0.2254(3)	0.5088(2)	39(2)
C(6)	0.2724(3)	0.3082(3)	0.5081(2)	39(2)
C(7)	0.2498(3)	0.3580(3)	0.4432(2)	44(2)
C(8)	0.3650(3)	0.3392(2)	0.5606(2)	36(2)
C(9)	0.5896(3)	0.2742(2)	0.6832(1)	32(2)
C(10)	0.6813(3)	0.3111(3)	0.7335(2)	38(2)
C(11)	0.6614(3)	0.4089(3)	0.7653(2)	46(2)
C(12)	0.5529(3)	0.4692(3)	0.7494(2)	47(2)
C(13)	0.4616(3)	0.4329(2)	0.7013(2)	40(2)
C(14)	0.4796(3)	0.3371(2)	0.6680(2)	32(2)
C(15)	0.5184(3)	0.0857(3)	0.6584(2)	37(2)
C(16)	0.6028(3)	0.1699(2)	0.6466(2)	36(2)
C(17)	0.6944(3)	0.1537(3)	0.5988(2)	40(2)
C(18)	0.6972(3)	0.0555(3)	0.5653(2)	53(2)
C(19)	0.6127(4)	−0.0256(3)	0.5772(2)	57(2)
C(20)	0.5226(3)	−0.0105(3)	0.6245(2)	51(2)
C(21)	0.1152(4)	0.2139(3)	0.9116(2)	65(2)
C(22)	0.4586(3)	−0.0491(3)	0.9106(2)	54(2)
C(23)	0.7896(3)	0.2396(3)	0.5836(2)	56(3)
C(24)	0.7984(3)	0.2460(3)	0.7557(2)	57(3)
C(25)	0.0064(4)	0.1632(3)	0.4223(2)	63(3)
C(26)	0.3154(4)	0.4540(3)	0.4174(2)	59(3)

[a] Estimated standard deviations in the least significant digit are given in parentheses. [b] U_{eq} is equal to $^1/_3$ of the trace of the orthogonalized $\mathbf{U}_{ij}$ tensor.

parameters were fixed for **1** but were refined for **4**. Scattering factors and anomalous dispersion terms were taken from ref 27. The largest peak heights from the final difference Fourier maps were 0.385 e $Å^{-3}$ for **1** and 0.294 e $Å^{-3}$ for **4**. An extinction correction was refined in both cases, but in each case the final refined value was zero (to four significant figures) and was thus negligible. A weighting scheme was used of the form $1/[\sigma^2(F_o)^2 + (0.1P)^2]$, where $P = (F_o^2 + 2F_c^2)/3$. Final fractional atomic coordinates for **1** and **4** are listed in Tables 2 and 3. Selected bond distances and angles are listed in Table 5.

Intensity data for a dark brown crystal of **5** (0.06 × 0.05 × 0.44 mm) were measured at the University of Adelaide on an Enraf-Nonius CAD4-*F* diffractometer operating at room temperature and employing Mo *K*α radiation (graphite monochromator, $\lambda = 0.7107$ Å). The ω:2θ scan technique was employed to measure data to a maximum Bragg angle θ of 25°; no significant decomposition of the crystal occurred during the data collection. Lorentz and polarization corrections were applied,[28] as was an analytical absorption correction[29] (maximum and minimum transmission factors of 0.973 and 0.887, respectively). Details of the crystallographic experiment and the structural computations are summarized in Table 1.

The structure of **5** was solved by interpretation of the Patterson map. After location of all of the atoms, the structure was refined by a full-matrix least-squares procedure based on *F*.[29] Scattering factors for neutral Ni (corrected for $\Delta f'$ and $\Delta f''$) were taken from ref 30; scattering

Table 3. Fractional Atomic Coordinates and Equivalent Isotropic Displacement Parameters ($Å^2 \times 10^3$) for **4**[a]

atom	*x*	*y*	*z*	U_{eq}[b]
Ni	0.2500	−0.0602(1)	0.7500	30(1)
S	0.2884(1)	0.1095(1)	0.8377(1)	41(1)
N(1)	0.3312(1)	−0.1955(2)	0.8272(1)	31(1)
N(2)	0.4360(1)	0.0318(2)	1.0789(1)	41(1)
N(3)	0.3847(1)	0.1131(2)	1.0083(1)	36(1)
C(1)	0.3475(1)	−0.3083(2)	0.7901(1)	32(1)
C(2)	0.2910(2)	−0.4178(2)	0.7541(1)	35(1)
C(3)	0.3141(2)	−0.5304(3)	0.7275(2)	47(1)
C(4)	0.3900(2)	−0.5315(3)	0.7346(2)	52(2)
C(5)	0.4438(2)	−0.4206(3)	0.7686(2)	50(2)
C(6)	0.4232(2)	−0.3086(3)	0.7969(2)	40(1)
C(7)	0.3845(2)	−0.1907(2)	0.9085(2)	33(1)
C(8)	0.3930(2)	−0.0857(2)	0.9615(2)	33(1)
C(9)	0.4414(2)	−0.0864(3)	1.0501(2)	37(1)
C(10)	0.3570(1)	0.0446(2)	0.9370(1)	32(1)
C(11)	0.4927(2)	−0.1999(3)	1.1099(2)	53(2)
C(12)	0.3612(2)	0.2460(2)	1.0196(1)	37(2)
C(13)	0.3412(2)	0.2594(3)	1.0763(2)	45(1)
C(14)	0.3212(2)	0.3865(3)	1.0905(2)	53(2)
C(15)	0.3892(2)	0.4985(3)	1.0473(2)	58(2)
C(16)	0.3384(2)	0.4847(3)	0.9904(2)	60(2)
C(17)	0.3609(2)	0.3577(3)	0.9767(2)	48(2)

[a] Estimated standard deviations in the least significant digit are given in parentheses. [b] U_{eq} is equal to $^1/_3$ of the trace of the orthogonalized $\mathbf{U}_{ij}$ tensor.

factors for the remaining atoms were those incorporated in SHELX-76.[29] Anisotropic displacement parameters were employed for all non-hydrogen atoms, and hydrogen atoms were included in the model at their calculated positions (C−H 0.97 Å) and assigned a common isotropic displacement parameter which was refined. A weighting scheme of the form $k/[\sigma^2(F) + |g|F^2]$ was employed. The final analysis of variance showed no special features, indicating that the weighting scheme had been appropriate. The largest peak height from the final difference Fourier map was 0.66 e $Å^{-3}$.

Final fractional atomic coordinates for **5** are listed in Table 4, and selected bond distances and angles are listed in Table 5. Full crystallographic details, anisotropic displacement parameters, hydrogen atom parameters, and bond lengths and angles for complexes **1**, **4**, and **5** have been reported as supporting information. Structure factor amplitudes are available from the authors.

Results and Discussion

Synthesis and Characterization. The pyrazole-based complexes **1**−**4** were prepared either by reacting the −SBu^t-protected precursor Schiff base ligand with nickel(II) chloride in refluxing 2-methoxyethanol, thereby releasing isobutene and causing simultaneous formation of the NiN_2S_2 chelate (in the case of **1**),[31] or by reacting the free, nonprotected ligand with nickel(II) acetate in ethanol/chloroform solution (in the cases of **2**−**4**). The mercaptobenzaldimine complex, **5**, was prepared either by reacting the coordinated mercaptobenzaldehyde ligand (formed *in situ* between nickel(II) acetate and 2-mercaptobenzaldehyde) with 2,2′-diamino-6,6′-dimethylbiphenyl or by reacting nickel(II) acetate with a solution of the preformed Schiff base ligand. The parent ions could be readily detected in the mass spectra of these complexes.

The ^{1}H NMR spectral shifts for $CDCl_3$ solutions of the complexes at 293.7 K are given in Table 6. The numbering scheme for complex **3** is shown in Figure 2. Isotropic shifts are calculated relative to the spectra of the zinc(II) analogs.[3] The mercaptobenzaldimine complex, **5**, shows no shift in the resonance positions compared to the Zn(II) reference, which establishes the sole presence of the diamagnetic planar form in solution. There are significant paramagnetic shifts in the

(27) *International Tables for Crystallography*; Kluwer Academic Publishers: Dordrecht, The Netherlands, 1992; Vol. C, Tables 4.2.6.8 and 6.1.1.4.
(28) PREABS and PROCES, data reduction programs for the CAD4 diffractometer, University of Melbourne, 1981.
(29) Sheldrick, G. M. SHELX-76, a program for crystal structure determination; University of Cambridge; Cambridge, England, 1976.
(30) *International Tables for X-Ray Crystallography*; Kynoch Press: Birmingham, England, 1974; Vol. IV, pp 99, 149.
(31) Becher, J.; Toftlund, H.; Olesen, P. H.; Nissen, H. *Inorg. Chim. Acta* **1985**, *103*, 167.

Table 4. Fractional Atomic Coordinates and Average Equivalent Isotropic Displacement Parameters ($Å^2 \times 10^2$) for **5**[a,b]

atom	*x*	*y*	*z*	U_{eq}[b]
Ni	0.36303(4)	0.11989(8)	0.33732(5)	274
S(1)	0.4036(1)	0.2821(2)	0.3808(1)	376
S(2)	0.2898(1)	0.2146(2)	0.3544(1)	421
N(1)	0.4272(2)	0.0233(5)	0.3436(3)	245
N(2)	0.3202(2)	−0.0057(5)	0.2838(3)	269
C(1)	0.4699(3)	0.2789(6)	0.3616(4)	295
C(2)	0.4966(3)	0.3911(8)	0.3623(5)	426
C(3)	0.5493(3)	0.3957(9)	0.3489(5)	471
C(4)	0.5768(3)	0.2928(8)	0.3355(4)	411
C(5)	0.5522(3)	0.1833(8)	0.3369(4)	350
C(6)	0.4977(3)	0.1760(7)	0.3494(4)	292
C(7)	0.4773(3)	0.0552(6)	0.3502(4)	287
C(8)	0.4195(3)	−0.1040(6)	0.3594(4)	253
C(9)	0.4347(3)	−0.1440(7)	0.4347(4)	324
C(10)	0.4276(3)	−0.2633(8)	0.4528(4)	405
C(11)	0.4037(3)	−0.3405(7)	0.3955(4)	350
C(12)	0.3871(3)	−0.3027(7)	0.3200(4)	308
C(12)′	0.3570(3)	−0.3866(7)	0.2626(5)	429
C(13)	0.3966(3)	−0.1817(6)	0.2997(4)	255
C(14)	0.3795(3)	−0.1313(6)	0.2201(4)	263
C(15)	0.4007(3)	−0.1662(7)	0.1521(4)	340
C(15)′	0.4447(3)	−0.2578(7)	0.1549(5)	482
C(16)	0.3795(4)	−0.1128(9)	0.0819(4)	500
C(17)	0.3399(4)	−0.0276(8)	0.0760(4)	440
C(18)	0.3195(3)	0.0070(8)	0.1425(4)	400
C(19)	0.3398(3)	−0.0440(6)	0.2126(3)	274
C(20)	0.2786(3)	−0.0579(7)	0.3019(4)	326
C(21)	0.2510(3)	−0.0198(8)	0.3653(4)	353
C(22)	0.2196(3)	−0.1036(8)	0.3976(5)	476
C(23)	0.1892(4)	−0.0711(11)	0.4544(6)	661
C(24)	0.1875(4)	0.0470(11)	0.4747(6)	661
C(25)	0.2169(3)	0.1331(9)	0.4427(5)	474
C(26)	0.2511(3)	0.0994(8)	0.3896(4)	376

[a] Estimated standard deviations in the least significant digit(s) are given in parentheses. [b] $U_{eq} = (8\pi^2/3)(U_{11} + U_{22} + U_{33})$.

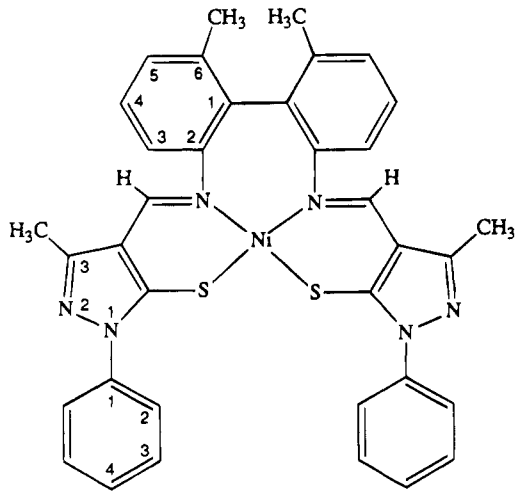

Figure 2. Numbering scheme for the ^1H NMR spectral assignments for complex **3**.

resonances in the pyrazole-based complexes, however, the most shifted resonance being due to the equivalent imine (CH=N) protons. The isotropic shifts of these and all other protons increases in the order **4** < **3** < **2** < **1**, with **1** showing an imine shift (148.52 ppm at 293 K) that is among the largest observed in four-coordinate Ni(II) complexes.[21]

The order of the isotropic shifts is that anticipated from the solid state magnetic and structural data (*vide infra*) and is consistent with the paramagnetic tetrahedral form becoming predominant in complexes **1** and **2**. Isotropic shifts are, in general, made up of contact and dipolar contributions, the latter essentially arising from magnetic anisotropy in the susceptibility tensor. Tetrahedral Ni(II) species, with $^3T_1$ ground states, would

Table 5. Selected Bond Distances (Å) and Angles (deg) in Complexes **1**, **4**, and **5**

	1	**4**	**5**
	Bond Lengths		
M–S(1)	2.240(1)	2.185(1)	2.152(2)
M–S(2)	2.244(1)		2.184(2)
M–N(1)	1.966(3)	1.927(2)	1.931(5)
M–N(2)	1.965(3)		1.917(6)
	Bond Angles		
N(1)–M–S(1)	100.1(1)	98.8(1)	95.3(2)
N(2)–M–S(2)	99.7(1)		89.2(2)
N(1)–M–N(2)	96.4(1)	93.5(1)	91.9(2)
S(1)–M–S(2)	117.6(1)	81.4(1)	85.3(1)
	Dihedral Angles		
N(1)–M–S(1)/N(2)–M–S(2)	77.4	35.7	14.4
N(1)–M–N(2)/S(1)–M–S(2)	74.5		14.8
	Biphenyl Twist Angle		
	66.8	49.5	61.6
	Bite		
N(1)···S(1)	3.226(3)	3.128(2)	3.021(6)
N(2)···S(2)	3.224(3)		2.886(6)
S(1)···S(2)	3.834(2)	2.850(1)	2.939(5)

be expected to display considerable anisotropy and hence involve dipolar contributions to the isotropic shifts.[32] However, it is evident even from the powder susceptibilities that the distortions from T_d symmetry in these $S = 1$ complexes lead to an orbitally nondegenerate ground state with little concomitant anisotropy. The shifts are therefore contact in origin, and this can also be seen in the alternating signs of the shifts noted for the biphenyl ring proton resonances (which arises from a π-spin-delocalization mechanism). Discussion of the temperature dependences of the isotropic shifts of the proton resonances for complexes **1**–**4** is given below, with particular emphasis on the estimation of thermodynamic parameters for the spin state equilibrium between planar ($S = 0$) and tetrahedral ($S = 1$) forms (formally $^1A_1 \rightleftarrows {}^3T_1$) occurring in chloroform solution. The relevant theoretical expressions are given in the Experimental Section and in ref 5. Discussion of the visible spectra of solutions of complexes **1**–**5** is given below.

Crystal Structures of Complexes 1, 4, and 5. The molecular structures of complexes **1**, **4**, and **5** are shown in Figures 3–5. Crystal packing diagrams show that these mononuclear NiN_2S_2 chelates are well separated from each other in the solid state. The coordination geometry in **1** is best described as distorted tetrahedral, while the coordination geometries of **4** and **5** are much closer to square planar. The dihedral angles between planes N(1)–Ni–S(1) and N(2)–Ni–S(2) (see Table 5) reflect these distortions. Thus, despite the influence of the (6,6′-dimethyl)biphenyl group, which tends to enforce a pseudotetrahedral geometry on the metal, the tendency of Ni(II) to prefer a *cis*-planar geometry with tetradentate ligands is dominant in **4** and **5**.

Interestingly, the Zn(II) analog of **1** has a similar pseudotetrahedral geometry with a dihedral angle of 75.3°.[3] This is in strong contrast to complex **5**, for which the corresponding Zn(II) derivative is again pseudotetrahedral, with a dihedral angle of 78.6°.[3] Two examples of Cu(II) complexes containing ligands of the bis(thiopyrazolyl)diphenyldiimine type exhibit intermediate distortions, with dihedral angles in the range 42–48°.[1,33] The biphenyl twist angle (*i.e.* the angle between the two phenyl planes when viewed along the C–C bond joining the rings) shows variations as the dihedral angle varies, although the range of variation (50–70°) is not large when compared to

(32) Bertini, I.; Sacconi, L.; Speroni, G. P. *Inorg. Chem.* **1972**, *11*, 1323.
(33) Hennig, L.; Kirmse, R.; Hammerich, O.; Larsen, S.; Frydendahl, H.; Toftlund, H.; Becher, J. *Inorg. Chim. Acta*, in press.

Table 6. ^{1}H NMR Resonance Positions (δ, ppm) and Isotropic Shifts ($\Delta\nu/\nu_0$, ppm (Relative to the Corresponding Zn(II) Complex) ($CDCl_3$, TMS Standard, 293.7 K; bp = Biphenyl, ph = Phenyl (at N1), pz = Pyrazole)

	1		2		3		4		5	
protons	δ	$\Delta\nu/\nu_0$	δ	$\Delta\nu/\nu_0$	δ	$\Delta\nu/\nu_0$	δ	$\Delta\nu/\nu_0$	δ	$\Delta\nu/\nu_0$
CH=N (2H)	156.64	148.52	117.96	109.90	66.63	58.45	48.6	40.77	7.57	−0.71
bp-3 (2H)	0.33	−6.76	2.45	−4.72	4.40	−2.68	5.45	−1.71	*b*	*a*
bp-4 (2H)	13.01	5.69	11.47	4.02	9.63	2.30	8.96	1.5	*b*	*a*
bp-5 (2H)	−0.61	−7.71	1.96	−5.37	4.14	−2.94	5.37	−1.1	*b*	*a*
bp-6 (2H)			9.79	2.55			8.20	0.8	*b*	*a*
ph-2 (4H)					8.99	1.36	8.64	1.2		
ph-3 (4H)					7.25	*a*	7.30	*a*		
ph-4 (2H)					7.53	*a*	7.47	*a*		
bp-6-CH_3 (6H)	0.21	−1.76			1.37	−0.61			2.12	0.14
pz-1-CH_3 (6H)	1.73	−1.92	2.18	−1.52						
pz-3-CH_3 (6H)	−3.36	−5.58	−2.04	−4.24	0.01	−2.26	0.63	−1.68		

[a] Shifts approximately zero. [b] δ values for the mercaptobenzaldimine and biphenyl aromatic protons lie in the range 6.90−7.66 ppm.

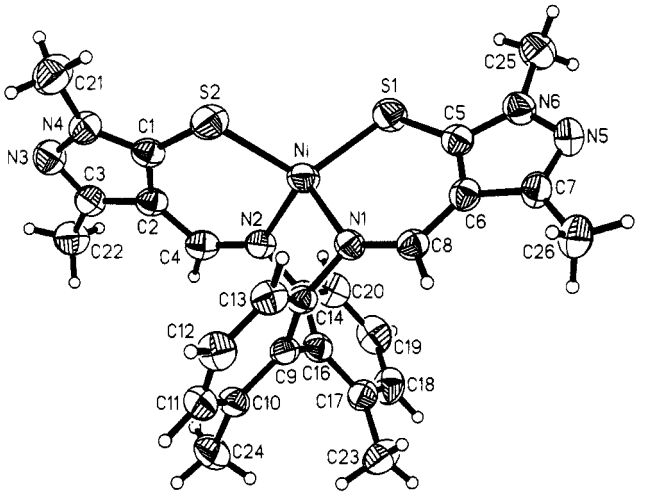

Figure 3. Molecular structure and crystallographic numbering scheme for **1**.

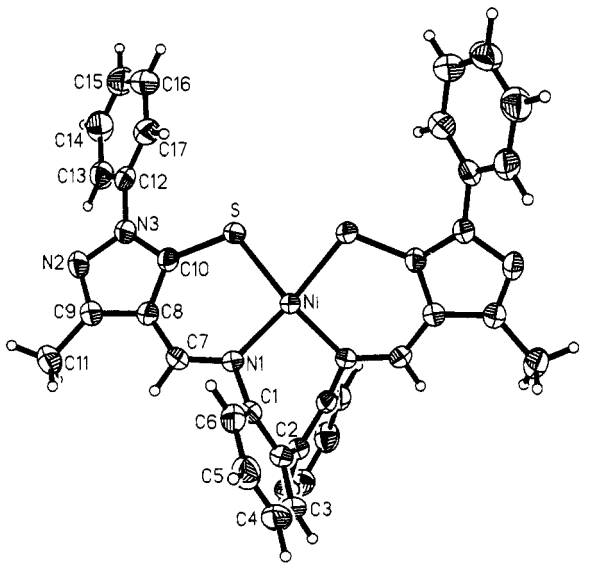

Figure 4. Molecular structure and crystallographic numbering scheme for **4**.

other biphenyldiimine metal complexes.[1,3,33−35] The incorporation of methyl groups at the 6 and 6′ positions also affects this twist angle to some degree. As the dihedral angle decreases from 77.4 to 35.7° on going from **1** to **4**, the twist angle decreases from 66.8 to 49.5°. The twist angle in **5** (61.6°) is smaller than it is in the Zn(II) analogue (70.2°).[3]

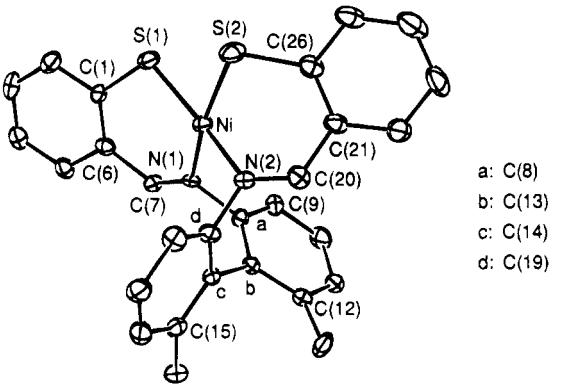

Figure 5. Molecular structure and crystallographic numbering scheme for **5**.

Other variations occur during these changes in coordination geometry. For instance, the "bite" distances N···S, N···N, and S···S vary in a reasonably straightforward manner. Thus, the average N···S bite decreases from **1** (3.226(3) Å) through **4** (3.128(2) Å) to **5** (2.95(1) Å) as the coordination geometry becomes less tetrahedral (*i.e.* more planar). The changes in the S···S distances are even more marked (3.834(2) Å in **1**, 2.850(1) Å in **4**, and 2.939(5) Å in **5**). This may reflect changes in S···S bonding, as well as steric effects.

Examination of the structures of other *cis*-N_2S_2 Ni(II) complexes containing *N,N*′-diaminoalkane backbones[13] reveals that the dihedral angles between the NiNS planes are generally in the range 0−38°. Angles near the top end of this range, which represent a higher degree of distortion from planarity, are found in the complexes containing the longer alkane chains. The recent work of Bereman *et al.*[14,15] showed that a gradual increase in the dihedral angle between the NiN_2 and NiS_2 planes occurred on changing from a $-N(CH_2)_2N-$ backbone (dihedral angle 3.4°) to a $-N(CH_2)_4N-$ backbone (dihedral angle 38.6°) in a homologous series of three *cis*-NiN_2S_2 complexes. Nivorozhkin *et al.* made similar observations[36] on two N-Pr^i-substituted pyrazolyl derivatives of the present kind of N_2S_2 system. In both of these studies, the complexes with tetramethylene chain backbones still possessed $S = 0$ ground states. It was only on going to a pentamethylene backbone that Nivorozhkin *et al.*[36] and Lippard *et al.*[16] (the latter reporting on aminotropocoronand NiN_4 complexes) found that a spin state change to $S = 1$ had occurred.

Comparison of dihedral angles with Ni−N and Ni−S bond distances may be done by examining the entries in Table 7, in which NiN_2S_2 complexes of all types (bis-bidentate or tetraden-

(34) Cheeseman, T. P.; Hall, D.; Waters, T. N. *J. Chem. Soc. A* **1966**, 1396.
(35) Pignolet, L. H.; Taylor, R. D.; Horrocks, W. deW., Jr. *J. Am. Chem. Soc.* **1969**, *91*, 5457.
(36) Nivorozhkin, A. L.; Konstantinovsky, L. E.; Nivorozhkin, L. E., Minkin, V. L.; Takhirov, T. G.; Diachenko, O. A.; Tagiev, D. B. *Izv. Akad. Nauk SSSR Ser. Khim.* **1990**, 327.

Table 7. Ranges of Ni–S and Ni–N Bond Lengths[a]

	Ni–S, Å	Ni–N, Å
cis-planar	2.12–2.18	1.85–1.95
tetrahedral	2.22–2.26	1.97–2.05
trans-planar	2.16–2.24	1.87–1.97

[a] Values taken from entries in the Cambridge Structural Database.

Table 8. Average Geometric Parameters within the Six-Membered Chelate Rings

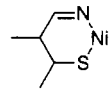

	S–C–C, deg	Ni–S–C, deg	N–Ni–S, deg	Ni–S, Å
1	131.1	104.1	99.9	2.24
4	128.2	107.4	98.8	2.18
5	124.4	106.1	92.2	2.16

tate, *cis*-planar (dihedral angle = 0°) or *trans*-planar (dihedral angle = 180°), etc.) are listed. Most of the complexes exhibit coordination geometries in the planar (dihedral angle = 0°) or pseudotetrahedral (dihedral angle = 75–100°) regions, although a number exhibit dihedral angles in the 0–75° range. The *trans*-NiN_2S_2 cases are all planar. It may be noted that the bond lengths in complexes **1**, **4**, and **5** fit within the appropriate ranges.

The changes in geometry within the six-membered chelate rings of complexes **1**, **4**, **5** and related NiN_2S_2 species may be correlated with the observed changes in spin state. While the bond distances in the chelate rings of **1** and **4** are consistent with the delocalized imine thiolato form of the ligands, the average values of the internal angles change as shown in Table 8. The C–C–S and S–Ni–N angles show the most marked differences among the three compounds **1**, **4**, and **5**. The Ni–S distance is slightly shorter in **5** than in **1** and **4**, but it should be noted that there are significant differences in the geometries of each half of the ligand in **5**. In particular, the Ni–S distances differ by 0.03 Å, while the N–Ni–S angles differ by 6.3° (see Table 5). Related, though less pronounced, differences were recently noted in a Ni(II) *N,N'*-trimethylene bis(cyclopentenedithiocarboxylate) complex, which exhibited a dihedral angle similar to that in **5**.[14,15] In that case, the asymmetry was ascribed to unequal interactions of the sulfur atoms with the metal d_π orbitals as a result of small distortions from planarity and to Ni–S covalency differences.

The puckering about the N···S axis may also be important in determining the geometry about the nickel(II) atom.[13,37,38] For example, in **5** the nickel atom is 0.55 Å above the best least-squares plane through S(1), C(1), C(6), C(7), and N(1) and 1.08 Å below the best least-squares plane through S(2), C(8), C(13), C(14), and N(2). This "stepped" structure, which is common in planar Schiff-base chelates,[39,40] leads to decreased steric repulsion between the biphenyl substituents on the coordinating nitrogen atoms. Some of the angles in the puckered ring are typical of the preferred *cis*-planar NiN_2S_2 coordination (about S, angles Ni–S–C of 109.6(3) and 103.0(8)°; about N, angles Ni–N–C of 130.8(6) and 130.8(6)°). A related (2-mercaptobenzaldiminato)nickel(II) complex (bis-bidentate Ni(mb-N-$C_6H_4N)_2$) has been shown[13] to display conformational features similar to those in **5**.

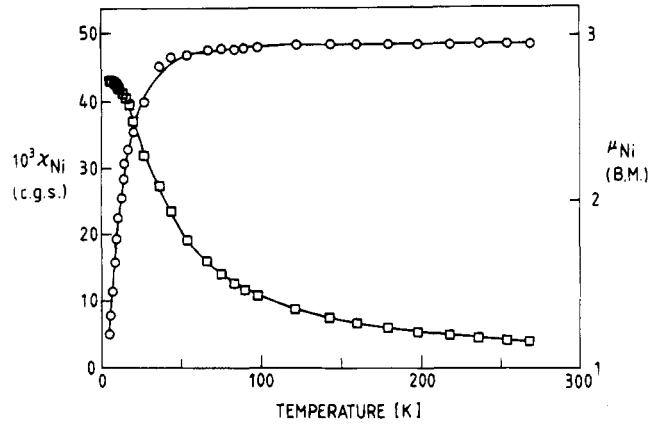

Figure 6. Plots of magnetic moment (○) and susceptibility (□) versus temperature for complex **1**. The solid lines are those calculated using eq 1 and the *D* value given in Table 9.

Table 9. Magnetic Moments and Zero-Field Splitting Parameters for **1**–**5**

		μ_{eff}, μ_B		
complex	color	(4.2 K)	(300 K)	D, cm^{-1}
1	brown	1.21	3.09	36
2	green	0.93	3.02	53
3	olive green	0.38	0.40	
4	olive green		0.36	
5	brown		0.58	

Solid State Magnetic Properties. The room-temperature magnetic moments of the complexes are summarized in Table 9. Complexes **1** and **2** have moments corresponding to high-spin ($S = 1$) d^8 systems, although the values are lower than those commonly found in tetrahedral species with symmetries close to T_d and a $^3T_1$ ground state. The consequences of these distortions from tetrahedral geometry are confirmed in the 4.2–300 K variable-temperature data, which show a constant value for μ_{Ni} between 300 K and 40 K and a rapid decrease between 40 K and 4.2 K; the limiting values are given in Table 9.

The observed behavior corresponds to the temperature dependence expected for an orbitally nondegenerate ^3A ground state which is well separated from the ^3E component (also derived from the $^3T_1$ state in, say, D_{2d} symmetry), and there is no evidence for any spin crossover behavior. Similar behavior was noted for some $S = 1$ Ni(II) tropocoronand complexes,[16] but no attempt was made to fit the magnetic data. The steep decrease in μ_{Ni} at low temperatures, which corresponds to a plateau in χ_{Ni}, arises due to zero-field splitting of the ^3A state into $M_s = \pm 1$ and $M_s = 0$ levels. The susceptibility plots for **1** and **2** could be fitted well to a simple spin Hamiltonian of the axial type (eq 1), even though the symmetry observed in the structural studies is not perfectly axial.

$$H = g\beta\mathbf{H}\cdot\mathbf{S} + D[S_z^2 + (^1/_3)S(S+1)] \qquad (1)$$

The best-fit plot of the data for complex **1** is shown in Figure 6. The *D* value of 34 cm^{-1}, which is reflected in the $\chi_{(0\ K)}$ plateau value of 0.042 $cm^3\ mol^{-1}$, is lower than that obtained for **2** (53 cm^{-1}), which has a $\chi_{(0\ K)}$ plateau value of 0.026 $cm^3\ mol^{-1}$. In both cases, the best-fit *g* values were 2.09. The *D* values for **1** and **2** are much larger than those commonly encountered for distorted octahedral Ni(II) complexes such as *trans*-$Ni(py)_4Cl_2$ ($D = 4.8$ cm^{-1}).[41] This is because spin–orbit coupling connects the two sublevels of the $^3T_1$ parent ground

(37) Kharabaev, N. N.; Kogan, V. A. *Dokl. Akad. Nauk. SSSR* **1985**, *282*, 396.
(38) Kharabaev, N. N. *Metalloorg. Khim.* **1990**, *3*, 1025.
(39) Calligaris, M.; Nardin, G.; Randaccio, L. *Coord. Chem. Rev.* **1972**, *7*, 385.
(40) Mistryukov, A. E.; Vasilchenko, I. F. ; Sergienko, V. S.; Nivorozhkin, A. L.; Kochin, S. G.; Porai-Koshits, M. A.; Nivorozhkin, L. E.; Garnovskii, A. D. *Mend. Commun*, **1992**, *1*, 30.
(41) Kennedy, B. J.; Murray, K. S.; Hitchman, M. A.; Rowbottom, G. L. *J. Chem. Soc., Dalton Trans.* **1987**, 285.
(42) Huang, Y.-H.; Kowal, A. T.; Moura, I.; Moura, J. J. G.; LeGall, J.; Adams, M. W. W.; Johnson, M. K. *J. Inorg. Biochem.* **1991**, *43*, 262.

state in the present systems whereas this is not the case for the $^3A_{2g}$ and $^3T_{2g}$ sublevels in the slightly distorted octahedral complexes. Somewhat similar values of D to those exhibited by **1** and **2** have recently been obtained from variable-temperature MCD studies on Ni(II)-substituted rubredoxin proteins; such systems presumably contain distorted tetrahedral $Ni(SR)_4$ centers.[42]

Complexes **3**−**5** are diamagnetic in the solid state, with room temperature μ_{Ni} values close to zero (0.36−0.58 μ_B). The structural studies showed that **4** and **5** exhibit coordination geometries close to planar (dihedral angles of 35.7 and 14.4°, respectively), and presumably **3** is similar to **4**. Planar d^8 systems are expected to exhibit small positive magnetic moments as a result of second-order Zeeman effects involving excited states.[43] Such effects should give a temperature-independent susceptibility value (TIP). Variable temperature measurements for **3** actually showed a Curie-like dependence of the weak susceptibilities (χ_{Ni} for **3** at 300 K of 6.6×10^{-5} cm^3 mol^{-1}), even allowing for errors in bucket calibration, ligand correction, etc. This behavior could arise either from a small amount (~1%) of an $S = 1$ impurity in the sample or from a small number of high-spin sites in the crystal lattice. Whatever the origin, the TIP contribution is very small in size. Indeed, other NiN_2S_2 complexes exhibit μ_{Ni} values intermediate in size (1.0−2.0 μ_B), and the origin of such values deserves further scrutiny.[44]

Electronic spectra. The absorption maxima of the nickel(II) complexes **1**−**5** in chloroform solutions within the spectral range 5000−40 000 cm^{-1} are reported in Table 10. Ligand field (LF), charge transfer (CT), and intraligand transitions are observed in each case. A typical spectrum is shown in Figure 7.

The pure low-spin complex **5** shows only two bands, which can be assigned as LF transitions. Complexes **1**−**4**, on the other hand, all show LF transitions both from the high-spin and the low-spin forms. The literature contains many examples that support the present assignments for the low-spin forms.[45] However, very few reliable studies on pseudotetrahedral Schiff base complexes have been reported. Gerloch *et al.*[46] carried out a single-crystal study on the bis(isopropylsalicylaldiminato)-nickel(II) complex and analyzed the data within the AOM model. Their assignments basically agree with those described below for **1**−**4**.

The low energy triplet state observed for the homologous series of high-spin forms of **1**−**4** ($^3A_2$) is a direct measure of the ligand field strength. Δ_T varies from 4420 to 4570 cm^{-1} along the series **1**−**4**, reflecting a slight increase in the donor properties of the ligands. The Δ_T values correlate straightforwardly with the low-spin population, but as **4** crystallizes in the low-spin form we cannot determine whether the variation of the ligand field strength in the high-spin series is due to structural changes. The position of the $^3T_1(P)$ transition, which mainly reflects the interelectronic Racah repulsion parameter B, remains remarkably constant through the series **1**−**4**, suggesting that no major changes in electronic delocalization occur. The observed B value of 770 cm^{-1} suggests a significant nephelauxetic effect for these complexes, as expected considering the high degree of electronic delocalization in these systems.[47]

Table 10. Electronic Spectra Absorption Maxima (cm^{-1}) and Molar Extinction Coefficients ϵ (in Parentheses) (M^{-1} cm^{-1}), in Chloroform

	$^3A_2$ (T_d)	^1D (T_d)	$^1B_{2g}$ (D_{4h})	$^3T_1(P)$ (T_d)	^1E_g (D_{4h})	CT (S → Ni)	intraligand transitions		
1	7950 (20.6)	10 500 (sh) (18)	14 300 (sh) (250)	17 300 (840)		23 700 (2500)	29 200 (sh) (10 000)	34 400 (sh) (28 000)	38 300 (37 000)
2	7970 (14.8)	10 500 (sh) (16)	14 300 (sh) (200)	17 300 (650)		23 300 (2400)	28 900 (sh) (10 000)	34 200 (sh) (31 000)	38 200 (47 000)
3	8150 (9.6)	11 000 (sh) (22)	14 400 (sh) (160)	17 300 (520)		23 100 (2500)	28 600 (sh) (12 000)	34 000 (sh) (45 000)	37 400 (50 000)
4	8220 (6.6)	11 000 (sh) (19)	14 400 (sh) (140)	17 300 (380)		23 100 (2200)	28 200 (sh) (11 000)		37 200 (52 000)
5			15 000 (sh) (150)		18 500 (sh) (1000)	23 600 (5100)		33 900 (sh) (33 000)	38 200 (47 000)

(43) Barraclough, C. G.; Martin, R. L.; Mitra, S. *J. Chem. Phys.* **1971**, *55*, 1426.
(44) Garnovskii, A. D.; Kurbatov, V. P.; Porai-Koshits, B. A.; Osipov, O. A.; Keifko, I. Y.; Minkina, L. S.; Sofina, G. M.; Soloshko-Dorosh, A. F. *J. Gen. Chem. USSR* **1970**, *40*, 2326.
(45) Lever, A. B. P. *Inorganic Electronic Spectroscopy*, 2nd ed.; Elsevier: Amsterdam, 1984.
(46) Cruse, D. A.; Gerloch, M. *J. Chem. Soc., Dalton Trans.* **1977**, 152.
(47) Jørgensen, C. K. *Modern Aspects of Ligand Field Theory*; North Holland Publ. Co.: Amsterdam, 1971.

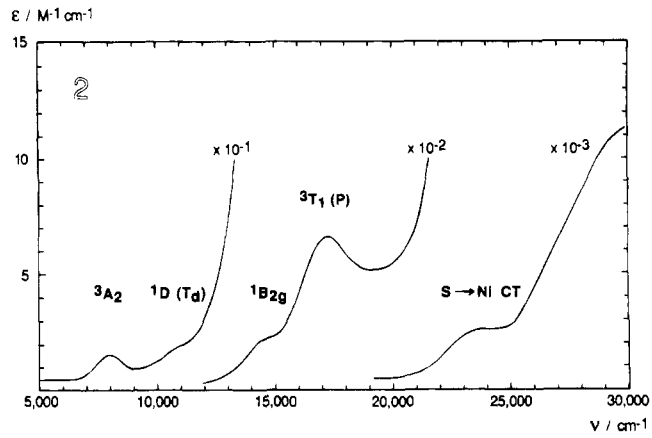

Figure 7. Electronic absorption spectrum of **2** in chloroform solution. The assignments of bands to the high-spin and low-spin forms are indicated.

An intense band around 23 000 cm^{-1} (ϵ = 2200–2500 M^{-1} cm^{-1}) is observed in all four cases. This band we assign as a LMCT transition. In the corresponding copper(II) complexes, similar bands are observed around 19 000 and 15 000 cm^{-1} (σ and π S → Cu(II)).[2] A comparison between ν_{obs} for Cu(II) and Ni(II) complexes can be made by using optical electronegativities.[47] By using the values of 2.2 and 2.4 as the optical electronegativities of Ni(II) and Cu(II) respectively, a value of 7300 cm^{-1} as the spin pairing energy of Ni(II) and a Δ value of 23 000 cm^{-1}, a blue shift of 6800 cm^{-1} is predicted for the LMCT transitions in low-spin Ni(II) complexes compared to Cu(II) complexes. On the basis of this analysis, the bands around 23 500 cm^{-1} are assigned as the π(S) → Ni(II) LMCT transitions of the low-spin forms. As the geometries differ considerably among the complexes, the agreement is not expected to be very good. The CT bands of the corresponding high-spin nickel(II) complexes are predicted to be further blue shifted.

While the σ component of the CT transitions is probably hidden under the intraligand transitions, the π component is observable. The position of the CT bands should correlate with the inner coordination sphere stereochemistry, as was the case in the corresponding Cu(II) complexes.[1,2] Surprisingly, the band position changes only to a very small extent within this series. The same observation was made for a series of alkane-strapped bis(methyl-2-amine-1-cyclopentenedithiocarboxylato) nickel(II) complexes.[14,15] In those complexes, changing the dihedral angle from 3.4 to 38.6° only changed the position of the CT band from 22 000 to 21 800 cm^{-1}.

Each of the complexes **1**–**5** exhibits a weak band around 14 500 cm^{-1}, which is typical of the $^1B_{2g} \leftarrow {}^1A_{1g}$ transition for square planar (D_{4h}) complexes.[45] It has been argued that the position of this band should correlate with changes in the distortion of the coordination geometry toward a pseudotetrahedral stereochemistry.[15] As the position of this band is constant in complexes **1**–**4**, it follows that the coordination geometries of the low-spin forms in solution are rather similar, with dihedral angles of approximately 20°.

Spin Equilibria in Solution. The thermodynamic parameters for the spin-state equilibrium ($^3T_1 \rightleftarrows {}^1A_1$) of complexes **1**–**4** in chloroform solution were investigated by using three methods: (1) variable-temperature magnetic susceptibility measurement (Evans's method);[23] (2) analysis of the temperature variation of the isotropic shifts in the ^1H NMR spectra;[21] (3) determination of the relative intensities of the ligand field transitions $^3A_2 \leftarrow {}^3T_1$ (see Figure 8) of the mixtures at room temperature (assuming a constant extinction coefficient for the high-spin component throughout the series).

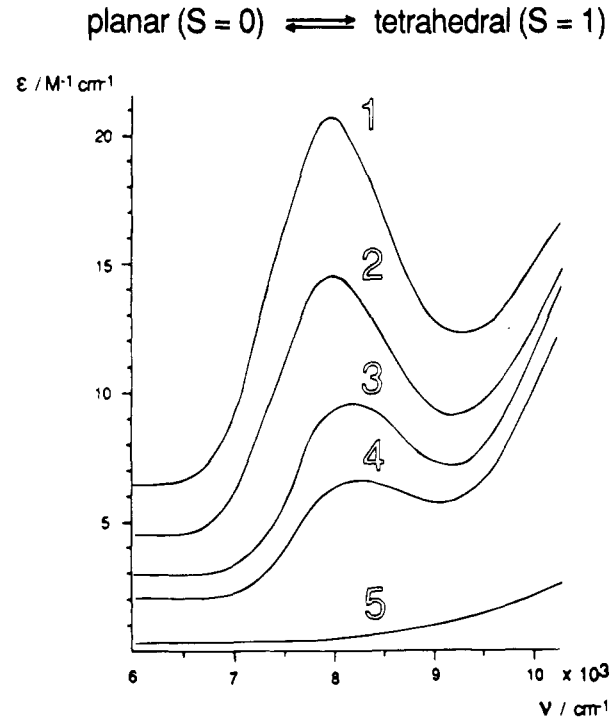

Figure 8. Electronic absorption spectra of **1**-**5** (in chloroform solution) in the near-infrared region. This absorption band is assigned to the $^3A_2 \leftarrow {}^3T_1$ transition of the high-spin form. The relative heights of the individual maxima provide good estimates of the high-spin population as purely low-spin complexes such as **5** do not absorb in this spectral region (see also Table 11).

The molar enthalpies and entropies of **1**–**3** were obtained from plots of the logarithm of the equilibrium constant, K_{eq}, versus $1/T$, as outlined in the Experimental Section. As shown in Table 11, the first two methods gave similar results. The third method only provides an estimate of the high-spin distribution at room temperature.

The critical temperature, T_c (K_{eq} = 1), is above room temperature for **1**–**5**. The values of ΔH and ΔS are similar to those found by Holm for a series of analogous NiN_2O_2 complexes.[5,6] The temperature-induced spin change is clearly an entropy-driven process, as ΔS is positive. The absolute value of the molar entropy is close to the statistical value for a distribution between singly degenerate ($^1A_1$) and ninefold degenerate ($^3T_1$) states (R ln 9 = 18.3 J mol^{-1}). Changes in solvation or in vibrational and rotational degrees of freedom had been expected to cause significant changes in ΔS, but these factors seem to be less important in the present series than in the analogous salicylaldimine complexes.[5,6]

All of the ^1H NMR signals can be assigned as a weighted average of contributions from high-spin and low-spin forms. This was also true for the low temperature spectra (down to 210 K), so the dynamics of the high-spin ⇄ low-spin equilibrium is not accessible by this technique for the present series of complexes. Similar results have been observed for other related systems.[5,6,15] However, the electronic spectra are clearly superpositions of high-spin and low-spin spectra. Therefore, the rate of spin change for these complexes must be in the range of 10^6 s^{-1} (based on $\Delta\nu$ = 150 ppm for the methine protons) to 10^{13} s^{-1} (from the near-IR spectra (see above)). Preliminary nanosecond flash experiments did not show any relaxation at room temperature, so the rates must be higher than 10^9 s^{-1}.[48]

Factors Determining the Spin State. Before attempting to rationalize the present results and place them in context, it is worthwhile to summarize briefly the general relations between

(48) McGarvey, J. J. Private communication, 1991.

Table 11. Thermodynamic Parameters for Complexes **1**−**5** ($\mu_{LS} = 0$)

	isotropic shift (imine H)		solution susceptibility			
	ΔH (kJ/mol) (ΔS (J/mol K))	ΔG (kJ/mol) (K_{eq} (293 K))	ΔH (kJ/mol) (ΔS (J/mol K))	ΔG (kJ/mol) (K_{eq} (293 K))	N_{HS} (293 K)	8000 cm^{-1} band ϵ_{corr}[a] (294 K)
1	8.26 (21.7)	1.90 (0.459)	8.20 (21.4)	1.92 (0.456)	0.313	11.2
2	9.56 (23.7)	2.63 (0.340)	9.56 (23.8)	2.59 (0.345)	0.257	7.9
3	11.7 (23.4)	4.86 (0.137)	12.4 (25.8[b])	4.84 (0.137[b])	0.121	4.3
4		5.70 (0.096)		6.15 (0.080)	0.074	2.4
5		- (~0)				~0

[a] Extinction coefficient of the pure high-spin component estimated by extrapolation to be *ca.* 35. Thus, for **1**, with $K_{eq} = 0.456$ a value of ϵ of ($^1/_3$)35 is predicted. The ϵ_{corr} values are also corrected for the background (see Figure 8). Observed ϵ values are given in Table 10. [b] Using data from the four highest temperatures only.

ligand type, coordination geometry, and spin state in NiN_2S_2 Schiff base systems containing six-membered chelate rings. Most tetradentate and bis-bidentate complexes containing mercaptobenzaldimine or mercapto-β-ketoimine ligands favor planar *cis*-N_2S_2 geometries and low-spin states for their nickel(II) complexes in the solid state and in solution.[5,12−14,32] Intramolecular S···S interactions are commonly advanced as the reason for the stabilization of this geometry.[1,49] Notable exceptions occur in sterically hindered *N-tert*-butyl bidentate complexes.[9,32]

The heterocycle-containing tetradentate ligands of the present pyrazole type, which contain *N,N'*-alkane bridges, fit into the low-spin category. However, bis-bidentate pyrazole- and pyrrole-based complexes favor a pseudotetrahedral high-spin configuration both in the crystalline state and in solution, even when small groups (such as methyl) are substituted on the imine nitrogen atom.[11−13] While the reasons for this are not yet clear, a subtle combination of steric effects brought about by the angle at the C−S carbon atom and electronic inductive effects at the coordinating nitrogen and sulfur atoms that derive from the presence of the pyrazole hetero-N atoms are probably responsible. Such factors are not, of course, present in the 2-mercaptobenzaldimine or mercapto-β-ketoimine systems.

All of the complexes in the present study contain a seven-membered chelate ring provided by a diaminobiphenyl moiety. It was expected that the nonplanarity of this moiety would provide enough sterically-driven twist to stabilize the high-spin pseudotetrahedral form of these nickel(II) complexes. This strategy apparently works in the solid state for the pyrazolyl-based systems **1** and **2**, but the pyrazolyl-based complexes **3** and **4** and the 2-mercaptobenzaldehyde-based complex **5** are low-spin even when the strongly twisted 6,6'-dimethylbiphenyl moiety is used as a backbone. As described in the structural discussion above, a number of steric effects favor a low-spin state for **4** and **5**.

For the homologous series of thiolatopyrazolylimine complexes, the high-spin fraction in solution increases from 0.074 for **4** to 0.313 for **1**. The pairs **1/2** and **3/4** only differ in the biphenyl backbone. As expected, the systems that have methyl groups in the 6 and 6' positions (**1** and **3**) have a larger high-spin population than the two systems (**2** and **4**) that only have protons in the 6 and 6' positions.

Surprisingly, the nature of the substituents on the pyrazolyl rings has a stronger influence on the spin state than does the nature of the substituents on the biphenyl moiety. A phenyl group on the pyrazole nitrogen atom, for example, favors the low-spin state compared with the complexes in which a methyl group occurs at this position. The molecular structures of complexes **1** and **4** do not indicate any intramolecular interaction between the two substituents in this position, so the trend must either have an electronic origin or be due to packing forces.

There is, indeed, a remarkable difference between the spin state distribution in the solid state and in chloroform solution for the two *N*-methyl-substituted complexes (**1** and **2**), both being high-spin (tetrahedral) in the solid and predominantly low-spin (square-planar) in solution. This change might be due to stabilization of the low-spin form by second-sphere interaction with chloroform solvent molecules. It should be noted that the positive ΔS value for the $^1A_1 \rightleftharpoons {}^3T_1$ interconversion in solution suggests a loss of solvent molecules in forming the high-spin form. The two *N*-phenyl-substituted complexes (**3** and **4**) are low-spin both in the solid state and in chloroform solution.

For a given ligand framework, it seems to be a general rule that bulky nonpolar and noninteracting substituents stabilize the low-spin form.[6,15] A striking example has been reported recently,[15c] in which a series of *trans*-bis-bidentate thiolato Schiff base complexes with different *N*-alkyl groups exhibited the highest proportion of high-spin population with the $N-C_2H_5$ substituent but a lower proportion with $N-C_3H_7$ and $N-C_4H_9$. In this connection, it should be pointed out that the local dielectric properties surrounding the coordination sphere have an important influence on the electrostatic potential about the central metal ion.[47] A low local dielectric constant tends to increase the ligand field strength as the compensating dielectric effect of the solvent is diminished.

The change in the spin state distribution in complexes **1**−**4** may also be influenced by electronic factors. Phenyl substituents extend the electronic delocalization of the ligand π systems, and the phenyl-substituted ligands may therefore serve as better π acceptors than the corresponding methyl-substituted ligands. A good π-accepting ligand stabilizes the low-spin form partly as a result of increased ligand field strength and partly as a result of decreased interelectronic repulsion.

Acknowledgment. This work has been supported by a grant from the Danish Natural Sciences Research Council (11-7783 to H.T., J.B., and H.F.). The data for Table 7 were kindly made available to us by Dr. Alan Hazell, Department of Chemistry, Aarhus University. The skilled assistance in NMR studies provided by Dr J. Weigold and in magnetic studies provided by Drs. C. D. Delfs and A. Markiewicz, all of the Department of Chemistry, Monash University, is gratefully acknowledged.

Supporting Information Available: For **1**, **4**, and **5**, a summary of X-ray analyses (Table S1), anisotropic displacement parameters (Tables S2, S5, and S8), hydrogen atom coordinates and *U* values (Tables S3, S6, and S9), and bond distances and angles (Tables S4, S7, and S10) (14 pages). Ordering information is given on any current masthead page. Structure factors for **1**, **4** and **5** available from the authors.

(49) Musker, W. K. *Acc. Chem. Res.* **1980**, *13*, 200.

IC9411312